Cr(VI) removal from aqueous solution using a magnetite snail shell

Le Phuong Hoang
Faculty of Civil and Environmental Engineering, Thai Nguyen University of Technology (TNUT), TichLuong Ward, Thai Nguyen, Vietnam.
Thi Minh Phuong Nguyen
Faculty of Environment and Chemical Engineering, Duy Tan University (DTU), 254 Nguyen Van Linh road, Da Nang, Vietnam.
Huu Tap Van
Faculty of Natural Resources and Environment, Thai Nguyen University of Sciences (TNUS), Tan Thinh ward, Thai Nguyen, Vietnam.
Thi Kim Dung Hoang
Faculty of Civil and Environmental Engineering, Thai Nguyen University of Technology (TNUT), TichLuong Ward, Thai Nguyen, Vietnam.
Xuan Hoa Vu
Institute of Research and Development, Duy Tan University, Da Nang 550000, Vietnam.
Tien Vinh Nguyen
Faculty of Engineering and IT, University of Technology Sydney (UTS), Box 123, Broadway, Sydney, PO, Australia.
N.X. Ca
Laboratory of Advanced Materials Chemistry, Advanced Institute of Materials Science, Ton Duc Thang University, Ho Chi Minh City, Vietnam
Faculty of Applied Sciences, Ton Duc Thang University, Ho Chi Minh City, Vietnam
Corresponding author: Email: nguyenxuanca@tdtu.edu.vn

Abstract

In this study, magnetic snail shell (MSS) prepared by impregnating of iron oxide onto snail shell (SS) powder was used for removing Cr(VI) from aqueous solution. Among 6 different mass ratios of Fe/SS powder studied, the MSS25 produced at a ratio of 25% achieved the highest Cr(VI) adsorption capacity. Batch adsorption experiments were conducted to investigate the adsorption isotherm, kinetics and mechanism of Cr(VI) onto MSS25. The results illustrated that adsorption of Cr(VI) onto MSS25 reached equilibrium after 150 min at pH 3. The adsorption kinetics could be well described by the pseudo-second order model (R^2=0.986). The Langmuir model (R^2=0.971) was the best-fitting model that described the adsorption isotherm of Cr(VI) onto MSS25. The maximum adsorption capacity was 46.08 mg Cr(VI) per gram of MSS25. Ion-exchange, electrostatic attraction and adsorption-coupled reduction were determined as the main adsorption mechanisms of Cr(VI) onto MSS25. The high percentages of $CaCO_3$ and Fe_3O_4 found in the MSS25 structure made a significant contribution to the Cr(VI) adsorption process.

Keywords: Cr(V) removal, magnetic snail shell, adsorption, low-cost adsorbent

1. Introduction

The discharge of industrial wastewater containing toxic heavy metals into the natural environment is one of the world's most serious pollution issues. Hexavalent chromium (Cr(VI)) is one of the most toxic heavy metals and has a lethal dose of only 0.1 mg/kg body weight. Drinking Cr(VI) contaminated water can lead to serious problems such as liver damage and pulmonary congestion (Karimi et al. 2012). Cr(VI) often exists in the effluents of industrial processes such as electroplating, leather tanning, textiles, mining, metallurgy and making fertilizer (Zhou et al. 2016). Therefore, it is necessary to remove Cr(VI) from wastewater before discharging it into the natural environment. Several technologies to remove Cr(VI) from industrial wastewaters have been reported such as ion exchange, electrolytic removal, adsorption, chemical precipitation, membrane filtration and solvent extraction (Bhaumik et al. 2013). Adsorption has been considered one of the most attractive methods due to its cost effectiveness, simplicity of operation and high removal efficiency, even when contaminants are in small concentrations in water environments (Mthombeni et al. 2018). Researchers have tried to find adsorbents which are low cost and have high adsorption capacity. Many natural adsorbents such as agricultural by-products (peanut hull, corncob, rice straw, walnut hell and mango kernel) (Inyang et al. 2016; Rai et al. 2016), biomass (*Spirulina maxima* and *Rhizopusnigricans*) (Bai R and Abraham 2001; Gong et al. 2005), and natural ore (zeolite; kaolinite) (Mthombeni et al. 2015; Turan et al. 2007) have been studied.

Biogenic calcium carbonate has been trialed successfully as a cost-effective biosorbent for heavy metals removal (Du et al. 2011; Hossain and Aditya 2013). Freshwater snail and mussel shells include 95%–99% calcite and/or aragonite (Hossain et al. 2015). They can be considered as potential cost-effective biosorbents due to their high calcium carbonate content. Some authors reported that their shell dust could effectively adsorb toxic metals (Du et al. 2011; Hossain and Aditya 2013; Van et al. 2018). The shell dust of the freshwater snail (*Lymnaealuteola*) can remove cadmium from aqueous solution with a high adsorption capacity of 16.66 mg/g being reported (Hossain and Aditya 2013). Mollusk shell powder was also documented for its effective removal of Pb, Cd and Zn from aqueous solutions with the epitaxial growth of otavite crystal on the surface of calcite (Du et al. 2011). In Vietnam and many countries in Asia, fresh snail is a very popular food source. A large amount of fresh snail shell is directly discharged into the

environment, which then causes odor issues. A new biosorbent produced from used snail shell can be an economical solution to: firstly, environmental pollution caused by heavy metals in aqueous environments; and secondly, manage used snail shells for other practical applications.

Recently, magnetic adsorbents have attracted more scientific attention due to their effective absorptivity and easy recovery of used materials after the treatment process (Han et al. 2016). These magnetic adsorbents can be synthesized by impregnating iron onto different materials such as biochar (Shang et al. 2016), activated carbon (Hao, Wang,Yan, Jiang, & Xu, 2018) or biomass (Akram et al. 2017), etc. However, to the best of our knowledge, no study has been done on combining snail shell and iron to produce a new magnetic material for Cr(VI) removal from aqueous solution. The aim of this study, therefore, was to: (i) develop a new absorbent namely magnetic snail shell (MSS) by impregnating iron oxide onto freshwater snail shell powder; and (ii) evaluate the performance of MSS on removing Cr(VI) from aqueous solution. The batch experiments under various operational conditions (pH, impregnation ratio of Fe and snail shell powder, concentrations of MSS and Cr(VI), contact time) were carried out to understand the behaviors of Cr(VI) adsorption onto MSS and to identify the adsorption mechanisms.

2. Materials and methods

2.1. Chemicals

All chemicals used in this study ($FeCl_3.6H_2O$, $K_2Cr_2O_7$, HCl and NaOH) were purchased from Merck (Darmstadt, Germany). The Cr(VI) stock solution (1000 mg/L) was prepared by dissolving 0.7024 g of potassium dichromate ($K_2Cr_2O_7$) in 250 mL double distilled water. Working Cr(VI) solutions with the desired concentrations were obtained by diluting the stock solution with double distilled water.

2.2. Preparation of magnetic snail shell

Snail shell (*Bellamyachinensis*) (SS) was collected from local restaurants in Thai Nguyen province, Vietnam. Snail shell was washed several times with tap water and distilled water to remove any adhering tissue portions. After cleaning with water, SS samples were air-dried (under sunlight) and then soaked in 0.1 M sulfuric acid solution for 8h and washed again with distilled water to remove any residual acid. The clean SS was then dried at 100^0C for 48h before it was crushed and sieved to a particle size of ≤ 0.5 mm for further experimentation.

Magnetic snail shell (MSS) was prepared according to the method employed by He et al. (2018) as follows. A predetermined amount of clean SS powder was soaked into the $FeCl_3$ solution of 100 g Fe/L with different mass ratios of Fe/SS powder, these being 0%, 5%, 10%, 15%, 20%, 25% and 30% (w/w). After agitating for 2h using magnetic stirrers, the mixtures were dried at 80^0C. The final dried products were marked as MSS0, MSS5, MSS10, MSS15, MSS20, MSS25 and MSS30, respectively, and stored in sealed bags before testing. MSS25 presented the best performance (details are presented in section 3.1) and so was chosen for the detailed characterization and batch experiments.

2.3. Characterization of magnetic snail shell

The morphological characteristics of clean SS, new MSS and MSS after absorption of Cr(VI) (MSS25-Cr) were determined by an energy dispersive X-ray spectroscopy equipped with EDS and SEM system (HITACHI S-4800), X-ray diffraction XRD-D8 ADVANCE with the Cu Ka radiation (λ = 1.54 Å). The functional groups of SS, MSS25 and Cr-MSS25 were identified by Fourier transform infrared spectroscopy (FTIR-6300) in the 500–4000 cm^{-1} range. The surface area (S_{BET}) of SS and MSS25 was determined by nitrogen adsorption/desorption isotherm at 77.35^0K (Coulter, USA). pH_{PZC} was determined via the common pH drift method (Zhao et al. 2016).

2.4. Batch adsorption experiments

Batch model experiment was conducted to evaluate the adsorption behavior of Cr(VI) on SS and MSS25 at different conditions, including impregnation ratio of Fe/SS (w/w) (0%, 5%, 10%, 15%, 20% and 25%), pH (2-12), contact time (5-240 min), adsorbent dose (10-120 mg/25 mL), and initial Cr(VI) concentration (5–80 mg/L). Batch experiments were conducted utilizing 50 mL Erlenmeyer flasks containing 25 mL of Cr(VI) solution. The initial pH of Cr(VI) solution was adjusted to a predetermined value by using HCl 0,1 M and NaOH 0,1M. The flasks were covered by paraffin before agitating them at 120rpm with a shaker (PH-2A, China). After the adsorption, the absorbent-absorbate mixture was separated by Whatman No. 1 filter papers (pore size of 11 μm). The total concentration of Cr(VI) remaining in the solution was determined by using Inductively coupled plasma-optical emission spectrometry (ICP-OES, Model: ULTIMA EXPERT, Horiba, France). The Cr(VI) amounts adsorbed onto MSS25 at any time t (q_t, mg/g) and equilibrium (q_e ,mg/g) were calculated by equations 1 and 2:

$$q_t = \frac{(C_o - C_t)V}{M} \quad (1)$$

where: C_0, C_t and C_e (mg/L) are concentrations of Cr(VI) in solution at the start, any time *t*, and equilibrium, respectively; V (L) is the volume of solution and M (g) is the dry weight of used adsorbent.

2.5. Adsorption kinetics

The pseudo-first-order, pseudo-second-order and Elovich models were used to analyze the experimental data in the kinetics study. The linear form of these three popular models can be written as follows, respectively:

$$\ln(q_e - q_t) = lnq_e - k_1 t \quad (2)$$

$$\frac{t}{q_t} = \frac{1}{k_2 q_e^2} + \frac{1}{q_e} t \quad (3)$$

$$q_t = \beta \ln(\alpha\beta t) \quad (4)$$

where:q_t (mg/g) and q_e (mg/g)is the adsorption capacity at time t (min) and at equilibrium, respectively; k_1(1/min) and k_2 (g/mg.min)are the rate constant of the pseudo-first-order and pseudo-second-order models, respectively; α (mg/g.min) is the initial adsorption rate; β (g/mg)is the adsorption constant.

2.6. Adsorption isothern models

The adsorption isotherm equilibrium provides useful data for explaining the adsorption mechanism. In this study, three adsorption isotherm models Langmuir, Freundlich and Temkin- were employed. The equations for these models are described below by Eqs (6), (7) and (8), respectively:

$$q_e = \frac{q_m K_L C_e}{1 + K_L C_e} \quad (5)$$

$$q_e = K_F C_e^{\frac{1}{n}} \quad (6)$$

$$q_e = \frac{RT}{b} \ln(A_T C_e) \quad (7)$$

where: q_m(mg/g) is the maximum adsorption capacity, C_e(mg/L) and q_e (mg/g) are the concentration of Cr(VI) in solution and adsorption capacity at equilibrium, respectively; K_L(L/mg): Langmuir constant; K_F(mg/g):Freundlich constant; n is the adsorption intensity; A_T (L/g): Temkin isotherm equilibrium binding constant; b: Temkin isotherm constant, R (8.314J/mol/K): universal gas constant; T: temperature at 298K.

3. Results and discussion

3.1. Optimizing the impregnation ratio of Fe and snail shell powder to produce MSS25

The first set of experiments was conducted by mixing 20 mg of MSS25 produced at different ratios of Fe and snail shell with 25 mL Cr(VI) solution of 10 mg/L at room temperature (25±2^{0}C). The amounts of Cr(VI) adsorbed by different magnetite SS are presented in Fig. 1.

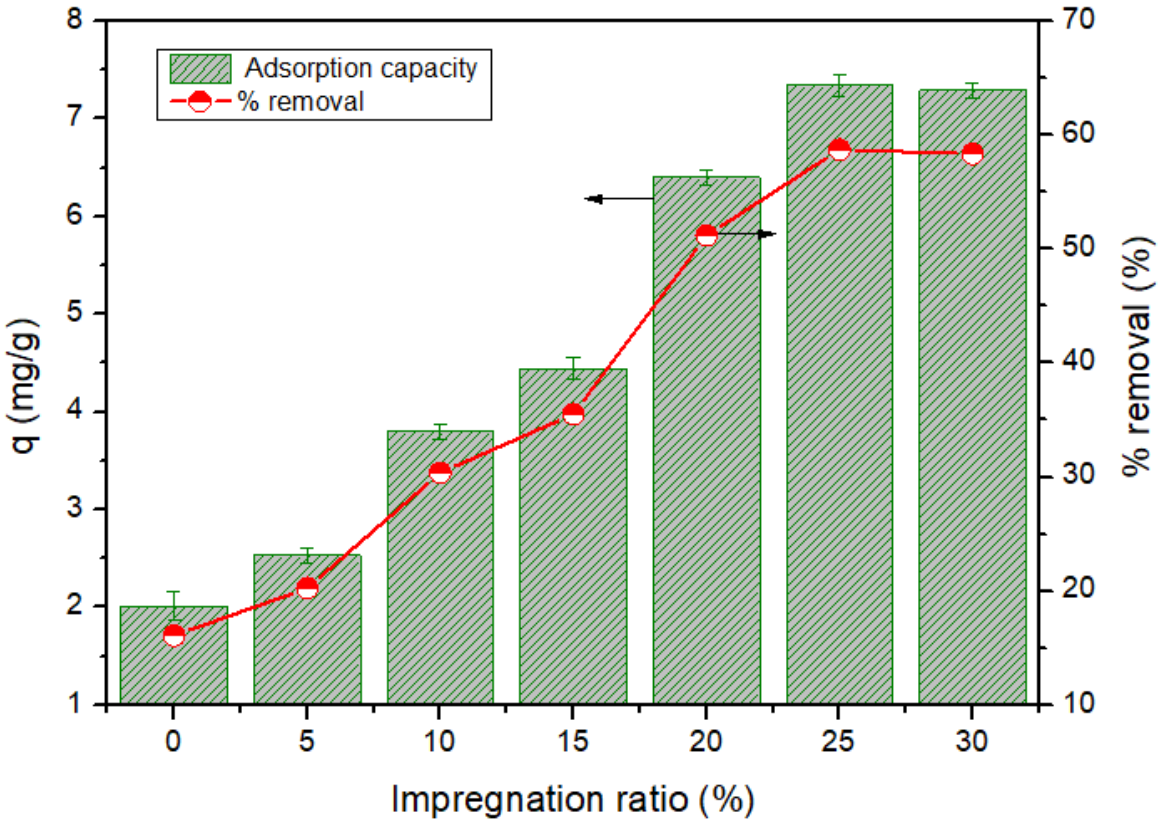

Fig. 1 The effect of the impregnation ratios of Fe/SS on Cr(VI) removal of MSS; Experimental conditions: initial Cr(VI) concentration: 10 mg/L, adsorbent dose: 20 mg/25 mL solution, contact time: 60 min

Results from Fig. 1 show that Cr(VI) adsorption capacity (q) and removal efficiency of MSS25 were higher than that of other MSS. The increase in the impregnation ratios of Fe and SS from 0 to 25% led to substantial improvements in

Cr(VI) adsorption capacity and removal efficiency, i.e. from 2.01 mg/g to 7.34 mg/g and from 16.07% to 58.73%, respectively. Lu et al. (2018) reported that Fe_3O_4 particles in the absorbent could form outer-sphere complexes with Cr(VI) and reduced Cr(VI) to Cr(III). However, when increase the impregnation ratio of Fe in SS to 30%, the removal efficiency of Cr(VI) only increased slightly to 58.93%. The trend of this result is similar to that of recent study of He et al. (2018). Their results indicate that Fe-impregnated biochar produced at a ratio of 30% did not significantly increase As removal efficiency compared to that produced at a ratio of 20%. Considering performance and economic factors, MSS25 produced at a Fe/SS ratio of 25% w/w was chosen for the subsequent experiments.

3.2. Characteristics of adsorbent

The BET surface area (S_{BET}) and total pore volume of SS were smaller than 2 m^2/g and 0.001 cm^3/g, respectively. After modification, both S_{BET} and total pore volume of MSS25 increased significantly to 69.69 m^2/g and 0.104 cm^3/g, respectively. The surface morphology and element composition of these adsorbents were shown in the results of SEM and EDS analyses. MSS25 possessed a more porous and rougher structure (Fig. 2b) than that of SS (Fig. 2a). Iron particles reacted with carbonate calcium ($CaCO_3$) led to the release of carbon elements and change in structure of the snail shell. Therefore, MSS25 was more porous and rougher structure than that of SS. This illustrates that iron oxide was successfully onto biochar's surface and caused a significant increase in surface are and pore volume (He et al. 2018). The EDS analysis results (Fig. 2d) indicated that SS was mainly composed of C (28.15%), O (62.28%) and Ca (9.57%) elements which revealed that the SS were mainly composed of crystalline $CaCO_3$ (Van et al. 2018). However, Fig. 2e depicts the proportions of elements for C, O, Cl, Ca and Fe in MSS25 were 6.05%, 70.84%, 9.31%, 6.64% and 7.16%, respectively. This indicated that iron oxide was successfully attached on SS's surface and this impregnation caused the difference between the surface of SS and MSS25. After MSS25 was used to adsorb Cr(VI) in solution, the Cr peaks appeared in the used MSS25 (Fig. 2f) and the surface morphology of MSS25-Cr was changed clearly (Fig. 2c). This clearly indicated the adsorption of Cr(VI) on the surface of MSS25.

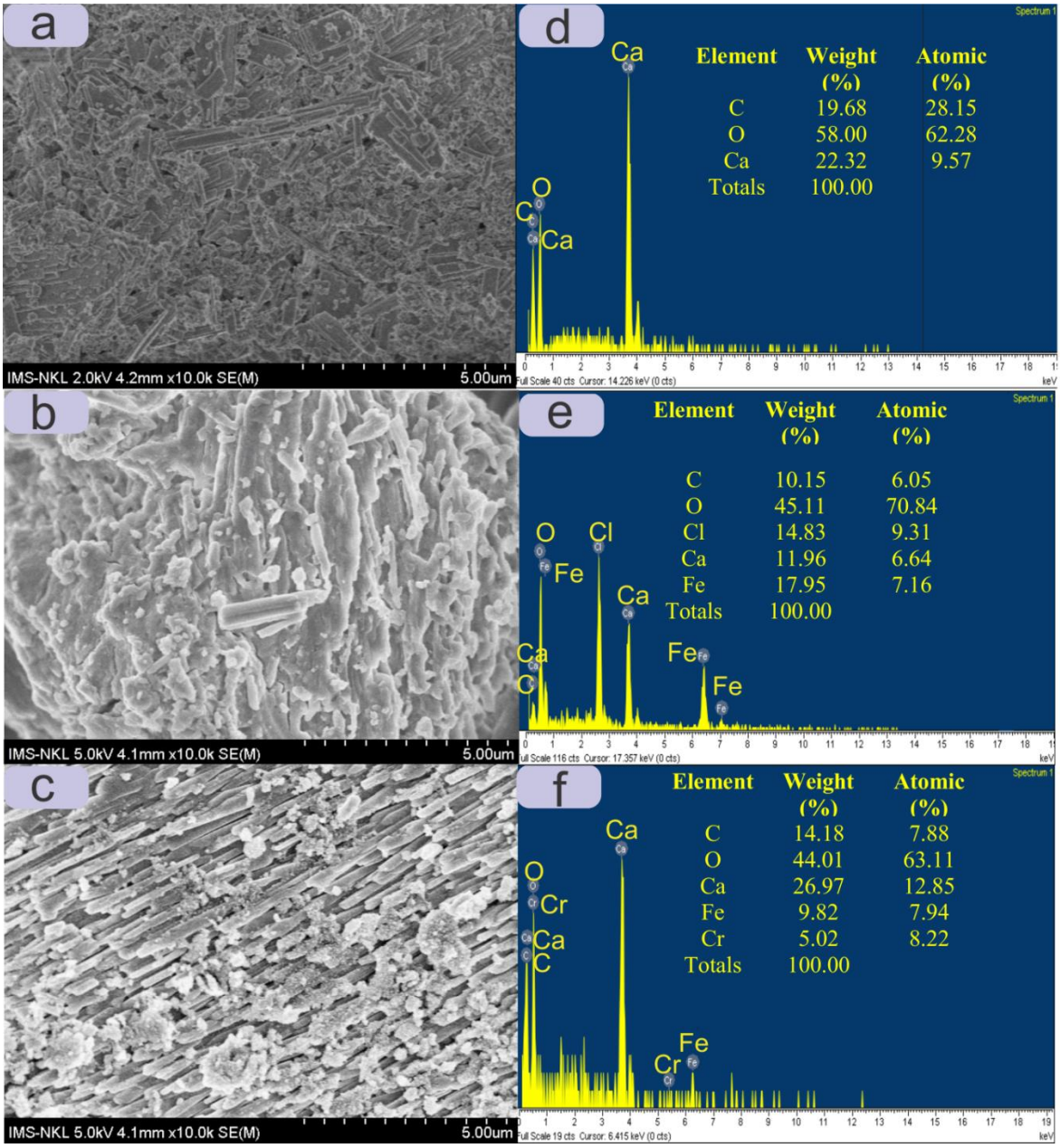

Fig. 2 SEM and EDS of (a, d)-snail shell (SS), (b, e)-magnetic snail shell (MSS25) and (c, f)-magnetic snail shell after Cr(VI) adsorption (MSS25-25)

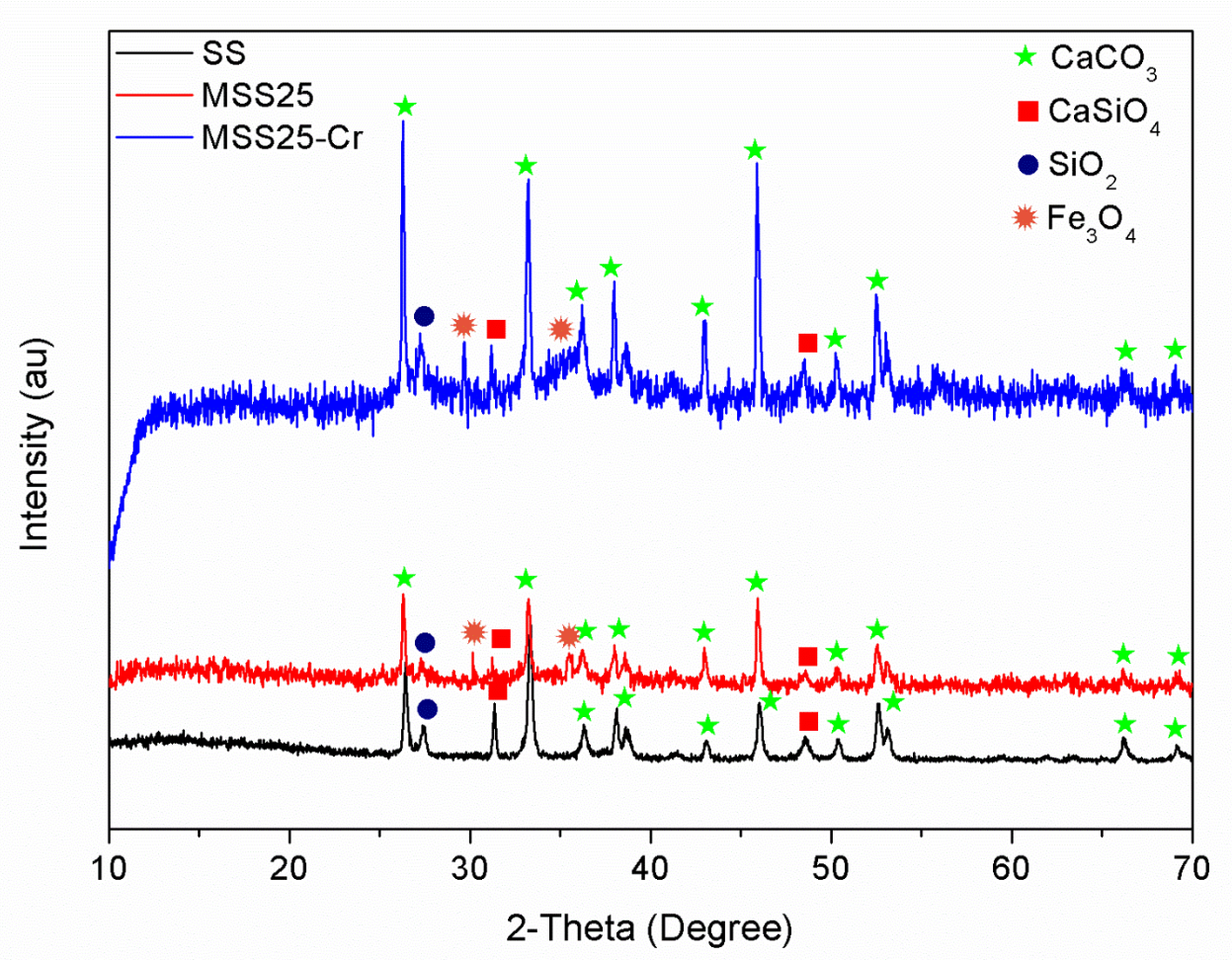

Fig. 3 XRD graphs of snail shell (SS), magnetic snail shell (MSS25) and magnetic snail shell after Cr(VI) adsorption (MSS25-Cr)

The XRD data also confirmed the presence of large amounts of $CaCO_3$ in SS. It suggests that SS is a biogenic aragonite (Fig. 4). In XRD patterns of MSS25, the appearance of new peaks at 30.0°, 35.5° and 63.1° were assigned as Fe_3O_4, respectively (Hu et al. 2017; Lu et al. 2018). These results further confirmed that Fe_3O_4 was successfully formed onto MSS25. Moreover, the dominant functional groups on the SS, MSS25 and MSS25-Cr surfaces were identified by the FTIR spectra (Fig. 4). A broad peak at around 3423 cm^{-1} was assigned to the vibration of O–H stretching. These peaks at approximately 1629 cm^{-1}, 1469 cm^{-1}, 1497 cm^{-1}, 857 cm^{-1} and 691 cm^{-1} contributed to the carbonate group's C-O stretching vibration (Van et al. 2018; Tizo et al. 2018). The characteristic bands at 1790 cm^{-1} and 1078 cm^{-1} involved the stretching vibration of C=O groups of carbonate ion (Nan et al. 2008; Tizo et al. 2018). This further confirms that calcite is the major constituent of SS powders. FTIR spectra of MSS25 and MSS25-Cr presented two new peaks at 1629 cm^{-1} and 1369 cm^{-1} in comparison with that of SS. Moreover, the peaks at 3423 cm^{-1} and 691 cm^{-1} became larger while the peak at 1497 cm^{-1} was narrower than that in SS.

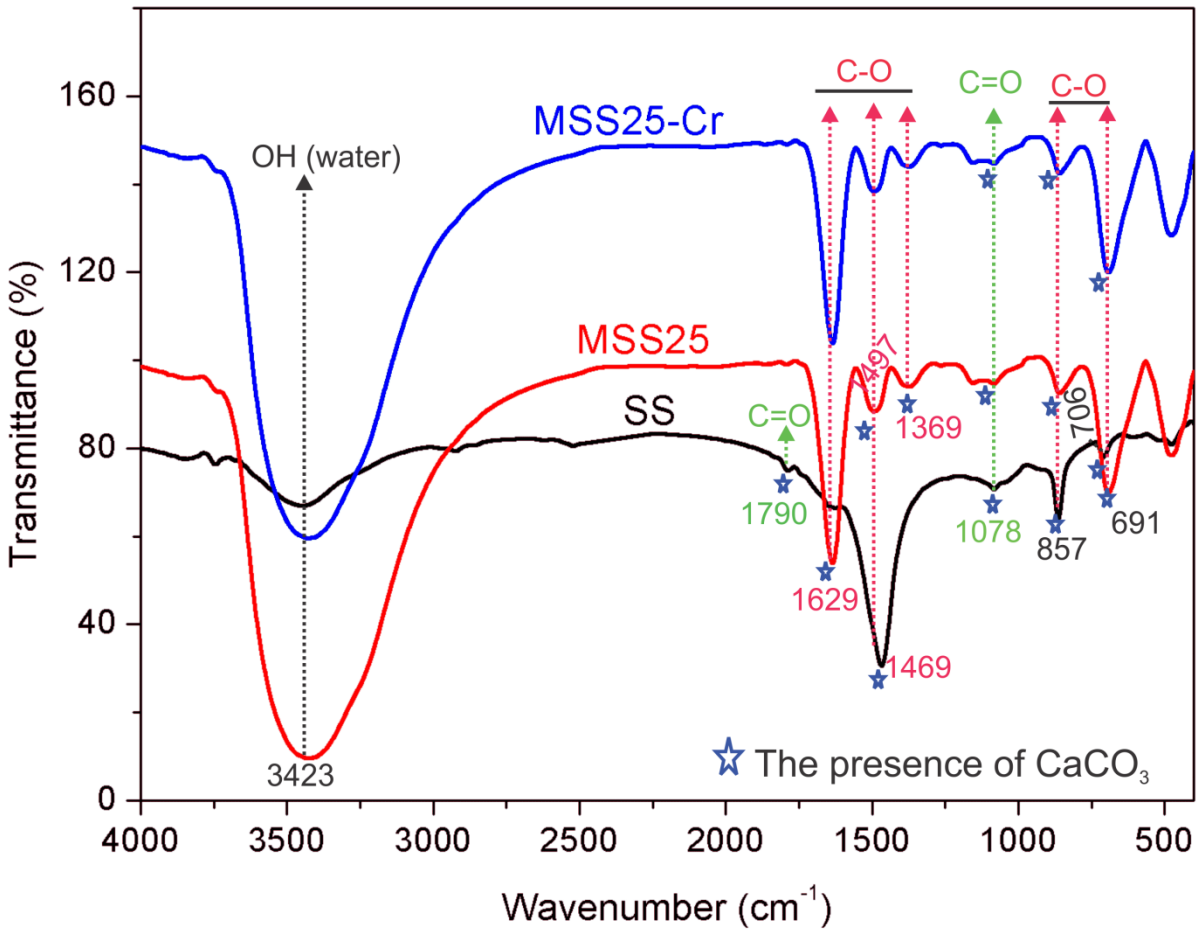

Fig. 4 FTIR graphs of snail shell (SS), magnetic snail shell (MSS25) and magnetic snail shell after Cr(VI) absorption (MSS25-Cr)

3.3 Effects of adsorption conditions on MSS25 performance

3.3.1. Effect of solution pH

The effect of pH of initial solution on Cr(IV) adsorption of MSS25 was investigated at different pH values, ranging from 2.0 to 10.0. The experiment was carried out at initial Cr(VI) concentrations of 10 mg/L, 20 mg/L and 30 mg/L, MSS25 dosage of 20 mg/25 mL solution and contact time of 60 min at room temperature (25 ± 2^0C). The experimental results are shown in Fig. 5a. It can be seen that adsorption capacity of Cr(VI) onto MSS25 decreased when solution pH increased. At pH from 2 to 3, the adsorption capacity of Cr(VI) reached the maximum values of 8.04 mg/g, 13.80 mg/g and 18.89 mg/g at initial Cr(VI) concentrations of 10 mg/L, 20 mg/L and 30 mg/L, respectively. Meanwhile, the Cr(IV) adsorption decreased sharply when pH values increased from 4 to 10 in all three initial Cr(VI) solutions. This decline can be explained as being due to: firstly, the effect of pH on the surface properties of the absorbent; and secondly, the forms of Cr ion in the solution (An et al. 2018; Chen et al. 2018; Zhou et al. 2016). In acidic conditions, Cr(VI) can be easily reduced to Cr(III) which is adsorbed better than Cr(VI) (Wang et al. 2014). As well, Cr(VI) mostly exists as $HCrO_4^-$ and $Cr_2O_7^{2-}$ at pH ranging from 2.0 to 6.4 and CrO_4^{2-} at pH > 6.4

(Chen et al. 2018; Zhou et al. 2016). The $HCrO_4^-$ contains less adsorption free energy (-2.5 to -0.6 kcal/mol) than CrO_4^{2-}(-2.1 to -0.3 kcal/mol). Subsequently, in the same conditions, CrO_4^{2-} is more difficult to remove than $HCrO_4^-$ (Shang et al. 2016).

Moreover, the zero point of charge (pH_{PZC}) of MSS25 was 7.51 (Fig. 5b). It means that when pH < pH_{PZC} (7.51), the surface of MSS25 was positively charged. This created significant electrostatic attraction with negatively charged chromate forms in the solution (Chen et al. 2018). Conversely, when pH > pH_{PZC} (7.51), the surface of MSS25 was negatively charged which hindered electrostatic force between the adsorbate and adsorbent (Akram et al. 2017). In addition, an increase in the solution pH led to an increase in the OH^- which could then compete with CrO_4^{2-} to occupy the active sites of MSS25 (Yang et al. 2018). Similar results have been reported in other studies (Akram et al. 2017; Shang et al. 2016). The results reported by Shang et al. (2016) showed that the maximum Cr(IV) adsorption onto biochar derived from herb-residue was achieved at pH 2. The optimal pH for the adsorption of Cr(VI) onto bio-composite of mango was reported at pH 3 (Akram et al. 2017).

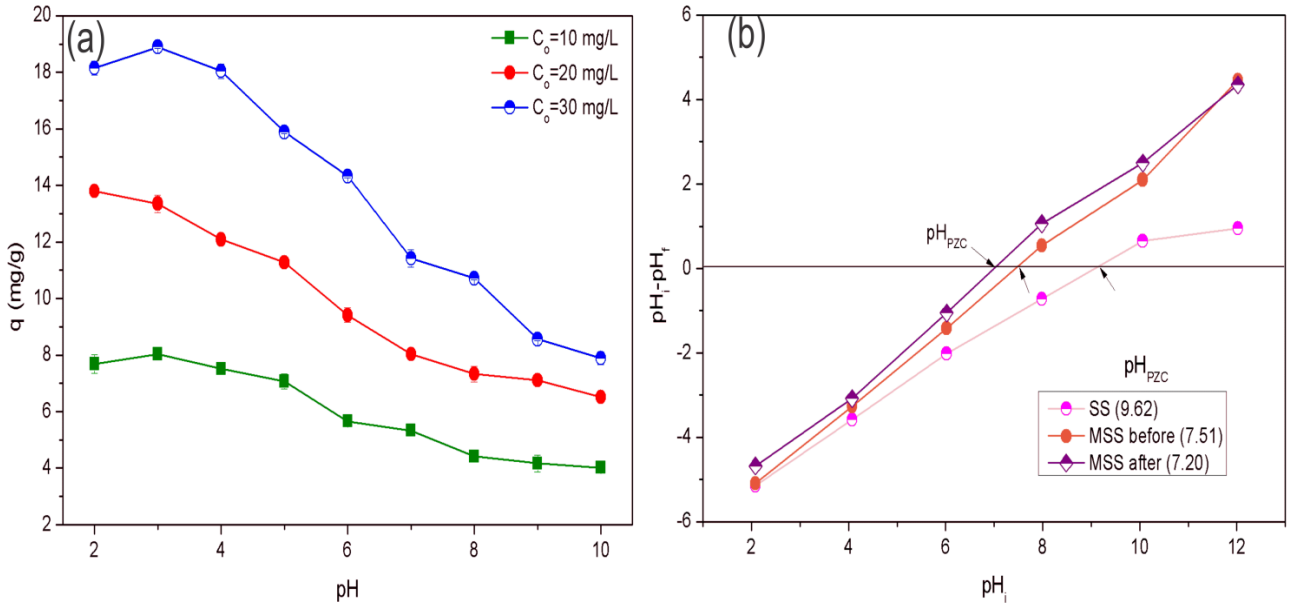

Fig. 5 (a) Effect of pH on the adsorption capacity of Cr(VI) onto MSS25 and (b) pH_{PZC} of MSS25. Experimental conditions: initial Cr(VI) concentrations: 10 mg/L, 20 mg/L and 30 mg/L; contact time: 60 min, adsorbent dose: 20 mg/25 mL

3.3.2. Effect of contact time

The effect of contact time on Cr(VI) adsorption was investigated at initial Cr(VI) concentrations of 10 mg/L, 20 mg/L and 30 mg/L, pH of 3.0, absorbent dose of 20 mg/25 mL solution and contact time ranging from 5 to 240 min. Fig. 6 shows that for the first 150 min, the Cr(VI) adsorbed onto MSS25 increased significantly, from 2.53 to 10.21 mg/g, 4.27 to 17.85 mg/g and 5.09 to 27.20 mg/g at initial Cr(VI) concentrations of 10 mg/L, 20 mg/L and 30 mg/L, respectively. The reason for this phenomenon is that a large number of active sites on the surface of the absorbent was available at the beginning (Deveci and Kar 2013). By further increasing the contact time from 150 to 240 min, the adsorbed amount increased slowly and remained unchanged due to the decline in the number of vacant sites

(Nguyen et al. 2019; Zhang et al. 2018). According to the results documented in this study, the contact time of 150 min was the best for removing Cr(VI) by MSS25 and therefore was used for the subsequent experiments. A similar equilibrium time of 150 min was also reported in one study of Cr(VI) adsorption on activated carbon prepared from mango kernel (Rai et al. 2016).

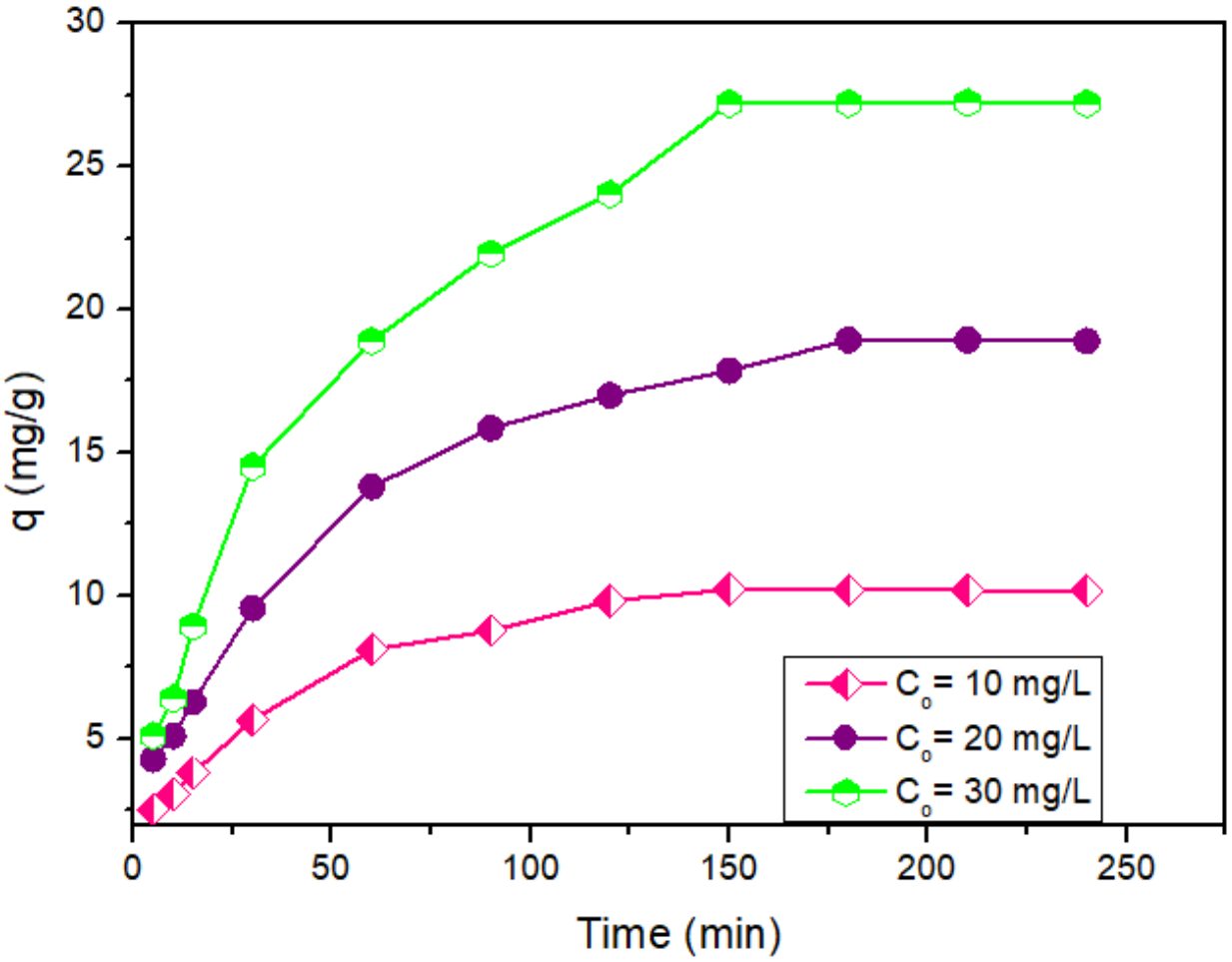

Fig. 6 Effect of contact time on Cr(VI) adsorption by MSS25; Experimental conditions: initial Cr(VI) concentration: 10 mg/L, 20 mg/L,30 mg/L; adsorbent dose: 20 mg/25 mL; pH: 3

3.3.3. Effect of absorbent dose

Adsorbent concentration has been considered to be a significantly factor determined the adsorbent-adsorbate equilibrium of the adsorption process (Deveci and Kar 2013; Xu et al. 2019). In this study, the dependence of Cr(VI) adsorption on MSS25 doses was conducted with the amount of adsorbent ranging from 10 to 120 mg/25mL, solution pH of 3, initial Cr(VI) concentration of 10 mg/L and contact time being 150 min. As seen in Fig. 7, the efficiency in removing Cr(VI) rose significantly from 35.51% to 94.28% when the MSS25 dose increased from 10 to 40 mg/25mL. It can be explained that with the increase of absorbent dose, the number of activate sites on FSS surface also rose and led to an increase in the binding sites for complexation of chromium ions (Bai R and Abraham 2001; Ertugay and Bayhan 2008). The experimental adsorption capacity reached the maximum value of 10.21 mg/g at the

dose of 20 mg/25m. However, when increasing the absorbent dose from 20 to 120 mg/25mL, the adsorption capacity fell sharply from 10.21 mg/g to 1.98 mg/g due to the overdose of adsorbent.

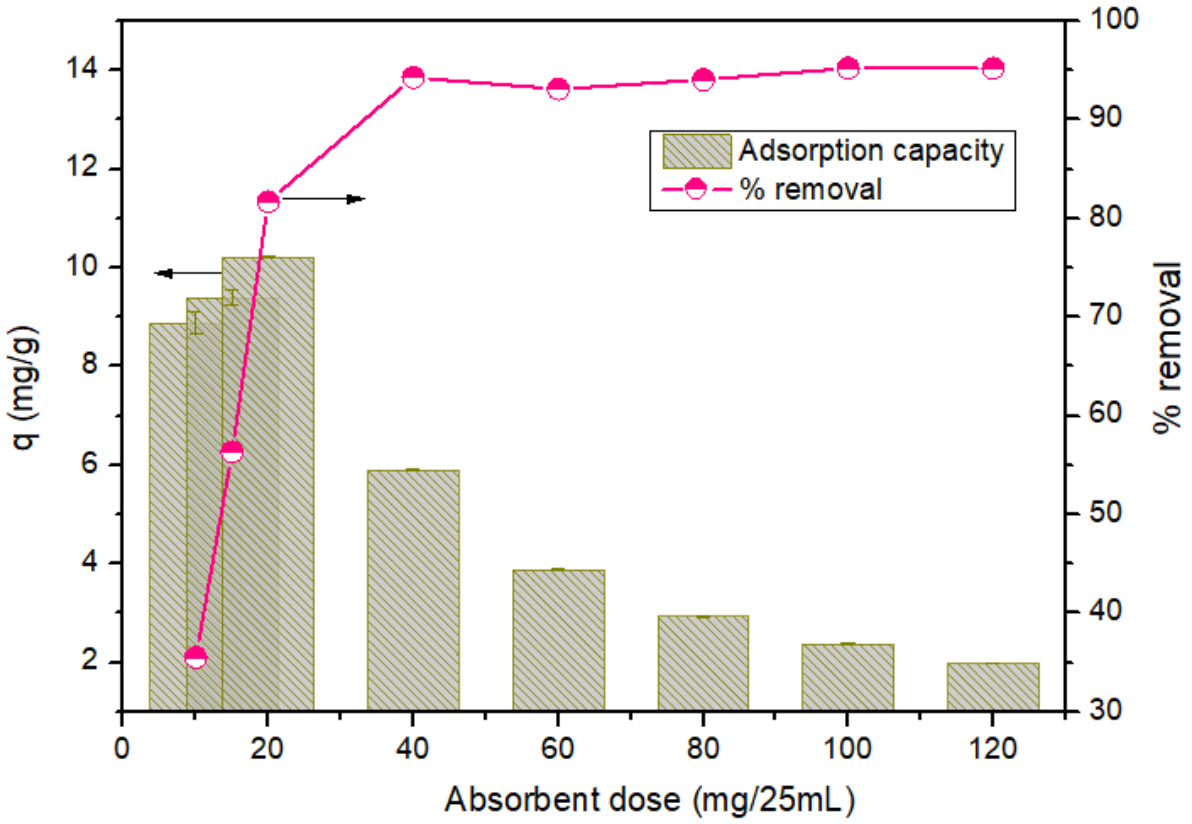

Fig. 7 Effect of adsorbent dosage on adsorption capacity and removal efficiency of Cr(VI) by MSS25; Experimental conditions: initial Cr(VI) concentration: 10 mg/L, contact time: 150 min, pH: 3

3.3.4. Effect of initial Cr(VI) concentration

The initial concentration is also an important factor in that it provides a vital driving force to overcome all mass transfer resistance of metal ion between the aqueous solution and absorbent (Dönmez and Aksu 2002). The effect of initial Cr(VI) ions concentration from 5 to 80 mg/L was investigated and results are shown in Fig. 8. It can be observed that adsorption capacity of Cr(VI) onto MSS25 increased from 5.75 mg/g to 39.09 mg/g when increasing the initial Cr(VI) concentration from 5 to 60 mg/L. However, at initial Cr(VI) concentration of more than 60 mg/L, the adsorption capacity did not increase any further. On the other hand, the amount of Cr(VI) removed fell from 92.03% to 39.17%, which corresponded to the increase of the initial Cr(VI) concentration from 5 to 80 mg/L. This can be explained by the increase of contact between activated sites on the absorbent's surface with adsorbate. After a certain level of increase in the initial Cr(VI) concentration, the available sites were occupied and saturated. Thus adsorption capacity of Cr(VI) reached stability (Rai et al. 2016). In addition, the ratio of available activated sites to Cr(VI) ions was lower at higher Cr(VI) concentration (Bai R and Abraham 2001). Consequently, the Cr(VI) removal efficiency decreased at the higher concentration. A similar trend on the role of initial Cr(VI) concentration in the adsorption process has been reported elsewhere such as research on removal of Cr(VI) from aqueous solutions using wheat shell (P. Das Saha et al. 2012) or walnut hull (X. S. Wang et al. 2009).

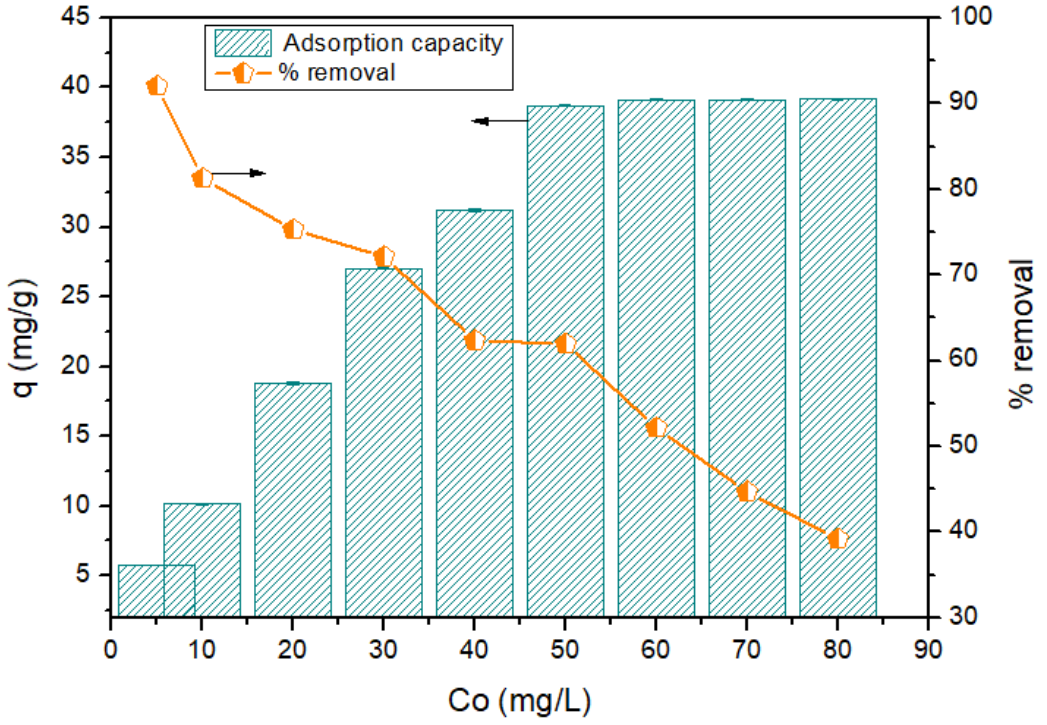

Fig. 8 Effect of initial Cr(VI) concentration on the adsorption capacity and removal efficiency when using MSS25; Experimental conditions: solution pH: 3, contact time: 150 min, adsorbent dose: 20 mg/25mL

3.3.5. Adsorption kinetics

The linear fitting kinetic parameters are summarized in Table 1 and Fig. 9. The linear regression coefficient R^2 values in the pseudo-first-order model, pseudo-second-order model and Elovich model were 0.975, 0.986 and 0.971, respectively. These results show that the Cr(VI) adsorption onto MSS25 fitted well with all three models. The pseudo-second-order model obtained the highest R^2 value. The calculated results of adsorption capacity derived from the pseudo-second order models (11.72 mg/g) were also close to the experimental data ($q_{e,exp}$ of 11.13 mg/g). This indicated two things: firstly, the pseudo-second-order model was the best fit for Cr(VI) removal by MSS25. It also indicated; and secondly, the adsorption of Cr(VI) onto MSS25 was a chemical sorption process.

Table 1. Kinetics parameters of models on Cr(VI) adsorption by MSS25

Pseudo-first-order			Pseudo-second-order			Elovich			$q_{e,exp}$ (mg/g)
$q_{e,cal}$ (mg/g)	k_1	R^2	$q_{e,cal}$ (mg/g)	k_2	R^2	α	β	R^2	
10.08	0.029	0.975	11.72	0.003	0.986	0.196	2.307	0.971	11.13

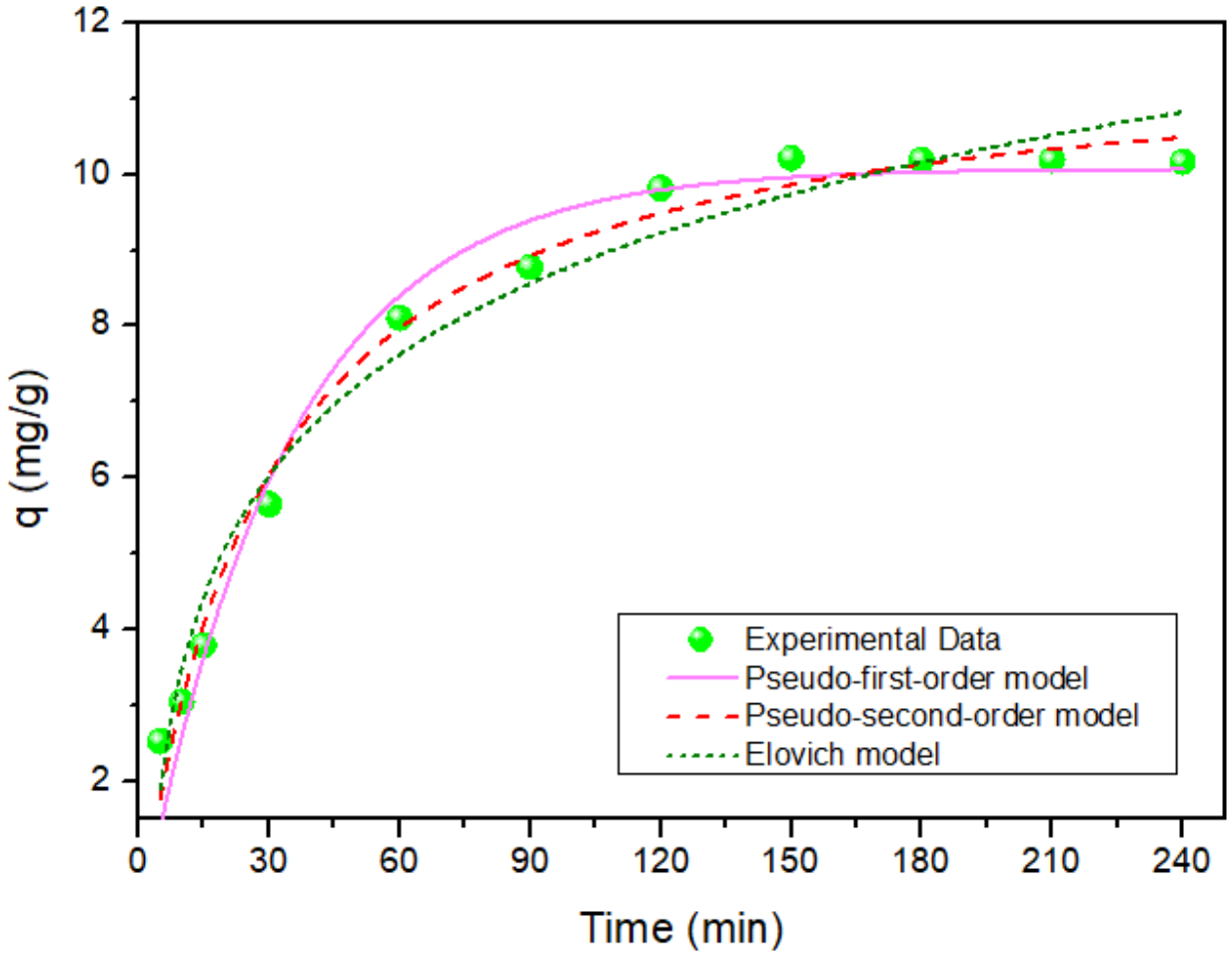

Fig. 9 Kinetics models of Cr(VI) adsorption onto MSS25; Experimental conditions: initial Cr(VI) concentration: 10 mg/L; adsorbent dose: 20 mg/25 mL; pH: 3; contact time: 150 min

3.3.6. Adsorption isotherm

The data obtained by fitting the three models are listed in Table 2 and their plots are shown in Fig. 10. With the highest R^2 values (0.971) and the minor difference between calculated q_m value (46.08 mg/g) and q_{exp} (39.17 mg/g), the Langmuir model is considered to be the best one for describing the adsorption of Cr(VI) onto MSS25. This suggested that the adsorption mainly occurred in the monolayer or through a fixed number of identical sites on the MSS25 surface. The adsorption also occurred at homogeneous adsorption sites of the MSS25 adsorbent (Shang et al. 2016). Furthermore, the 1/n value (0.339) obtained from the Freundlich model was below 1, which meant that the adsorption of Cr(VI) on MSS25 was favorable (Yuan et al. 2009).

Table 2 The adsorption isothermal parameters of Cr(VI) onto MSS25

Langmuir model			**Freundlich model**			**Temkin model**			**q_{mexp} (mg/g)**
q_m (mg/g)	K_L	R^2	K_F	1/n	R^2	A_T	b	R^2	
46.08	0.163	0.971	11.790	0.339	0.904	34.749	304.725	0.931	39.17

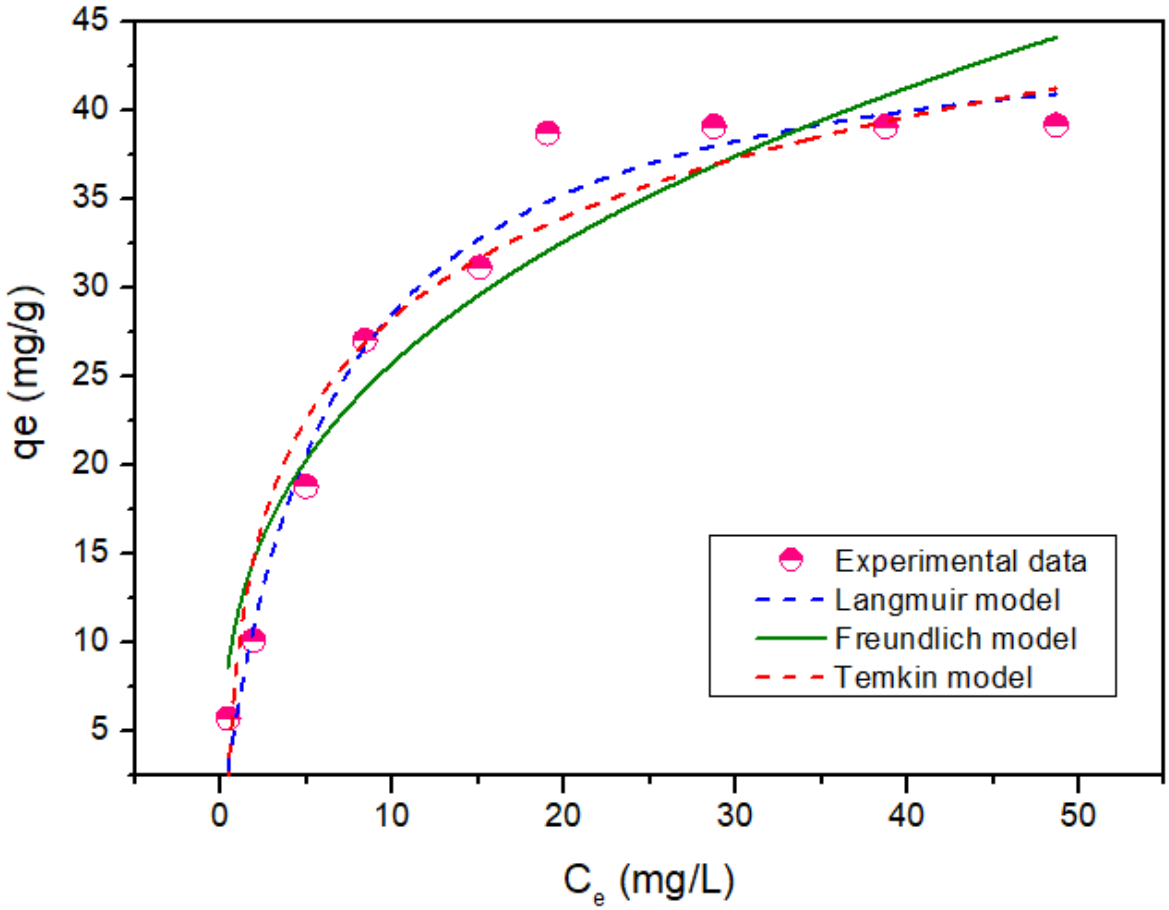

Fig. 10 Adsorption isotherm of Cr(VI) onto MSS25; Experimental conditions: adsorbent dose: 20 mg/25 mL; pH: 3; contact time: 150 min

3.3.7. Adsorption mechanism

The adsorption mechanism of toxic metals onto carbonate-rich materials was controlled by (1) pore filling, (2) electrostatic attraction (out-sphere complexes), (3) non-electrostatic attraction (inner-sphere complexation), (4) surface precipitation and (5) cation exchange (Alidoust et al. 2015). In this study, the adsorption mechanisms of Cr(VI) were also affected by the surface properties of MSS25. As previously discussed, the MSS25 adsorbent exhibited a higher S_{BET} value (69.69 m^2/g) than SS (< 2 m^2/g). Moreover, the analyses on the effects of pH show that the main adsorption of Cr(V)) occurred in acidic conditions and electrostatic attraction played an important role in binding Cr(VI) from the solution. Furthermore, anion exchange between Cr^{6+} oxyanions and Cl^- (Khitous et al. 2016) on the MSS25 did occur.

It can be observed for the EDS result in Fig. 2e (before adsorption) and Fig. 2f (after adsorption) that Cl^- was replaced by Cr^{6+}. The XRD patterns of MSS25 after adsorption revealed the changes in the MSS25 crystal structure. These results indicated that the CO_3^{2-} groups and carbonate-like species in $CaCO_3$ were replaced by anionic Cr(VI) species (CrO_4^{2-}). Moreover, Cr(VI) could be reduced to Cr(III) with the assistance of π electrons on the carboxyl groups of MSS25 (peak of 1790 and 1078 cm^{-1} in the FTIR result; see Fig. 3). Electrostatic repulsion between the

protonated hydroxyl groups occurred. Cr(III) cations was then adsorbed on MSS25 surface through substitution of Fe^{3+} with Cr^{3+} in the acidic state, complexation and formation of $Cr(OH)_3$ (Zhou et al. 2018). The reduction of Cr(VI) to Cr(III) in acidic conditions through equations (8) and (9) written below. XRD data of MSS25-Cr also confirmed that a crystal structure formed after the reaction process with Cr(VI). Cr(VI) might also be adsorbed through the charge imbalance, vacancies, and generation of chemical bonds due to the magnetic Fe_3O_4 on the surface of MSS25:

$$3Fe^{2+} + HCrO_4^- + 7H^+ \rightarrow 3Fe^{3+} + 4H_2O + Cr^{3+} \quad (8)$$

$$CrO_4^{2-} + 8H^+ + 3e^- \leftrightarrow Cr^{3+} + 4H_2O \quad (9)$$

4. Conclusion

Magnetic snail shell (MSS25) is a promising adsorbent for removing Cr(VI) from aqueous solutions due to its low cost and good performance. MSS25 was prepared by a simple process and the adsorption process reached a fast equilibrium at 150 min. In this study, the MSS25's adsorption capacity of Cr(VI) reached its peak in acidic conditions at pH of 2-3. The physico-chemical properties data indicated that $CaCO_3$ and Fe_3O_4 were distributed uniformly on the MSS25 surface. Our results demonstrated that the maximum adsorption capacity of Cr(VI) by MSS25 significantly increased after magnetization and the Langmuir maximum adsorption capacity of MSS25 was 46.08 mg Cr(VI)/g MSS25 at initial Cr(VI) concentration of 60 mg/L. The pseudo-second-order model fitted the best to this study's experimental data. Cr(VI) was adsorbed on MSS25 via ion exchange, electrostatic attraction and adsorption-coupled reduction. The highly efficient removal of Cr(VI) by MSS25 were helped by large amounts of $CaCO_3$ and Fe_3O_4 on MSS25.

Acknowledgments

The authors would like to acknowledge the financial support given by Thai Nguyen University of Technology (TNUT) and Thai Nguyen University under grant number DH2019-TN02-04.

References

Akram, M., Bhatti, H. N., Iqbal, M., Noreen, S., & Sadaf, S. (2017). Biocomposite efficiency for Cr(VI) adsorption: Kinetic, equilibrium and thermodynamics studies. *Journal of Environmental Chemical Engineering*, *5*(1), 400–411. doi:10.1016/j.jece.2016.12.002

Alidoust, D., Kawahigashi, M., Yoshizawa, S., Sumida, H., & Watanabe, M. (2015). Mechanism of cadmium biosorption from aqueous solutions using calcined oyster shells. *Journal of Environmental Management*, *150*, 103–110. doi:10.1016/j.jenvman.2014.10.032

An, Q., Li, X. Q., Nan, H. Y., Yu, Y., & Jiang, J. N. (2018). The potential adsorption mechanism of the biochars with different modification processes to Cr(VI). *Environmental Science and Pollution Research*, *25*(31), 31346–31357. doi:10.1007/s11356-018-3107-7

Bai R, S., & Abraham, T. E. (2001). Biosorption of Cr (VI) from aqueous solution by Rhizopus nigricans. *Bioresource Technology*, *79*(1), 73–81. doi:https://doi.org/10.1016/S0960-8524(00)00107-3

Bhaumik, M., Setshedi, K., & Maity, A. (2013). Chromium (VI) removal from water using fixed bed column of

polypyrrole/Fe_3O_4 nanocomposite. *Separation and Purification Technology*. doi:10.1016/j.seppur.2013.02.037

Chen, Y., Wang, B., Xin, J., Sun, P., & Wu, D. (2018). Adsorption behavior and mechanism of Cr(VI) by modified biochar derived from Enteromorpha prolifera. *Ecotoxicology and Environmental Safety*, *164*, 440–447. doi:https://doi.org/10.1016/j.ecoenv.2018.08.024

Deveci, H., & Kar, Y. (2013). Adsorption of hexavalent chromium from aqueous solutions by bio-chars obtained during biomass pyrolysis. *Journal of Industrial and Engineering Chemistry*, *19*(1), 190–196. doi:10.1016/j.jiec.2012.08.001

Dönmez, G., & Aksu, Z. (2002). Removal of chromium(VI) from saline wastewaters by Dunaliella species. *Process Biochemistry*, *38*(5), 751-762 doi:10.1016/S0032-9592(02)00204-2

Du, Y., Lian, F., & Zhu, L. (2011). Biosorption of divalent Pb, Cd and Zn on aragonite andcalcite mollusk shells. *Environmental Pollution*, *159*(7), 1763-1768. doi:10.1016/j.envpol.2011.04.017

Ertugay, N., & Bayhan, Y. K. (2008). Biosorption of Cr (VI) from aqueous solutions by biomass of Agaricus bisporus. *Journal of Hazardous Materials*, *154*(1-3), 432-439. doi:10.1016/j.jhazmat.2007.10.070

Gong, R., Ding, Y., Liu, H., Chen, Q., & Liu, Z. (2005). Lead biosorption and desorption by intact and pretreated spirulina maxima biomass. *Chemosphere*, *58*(1), 125-130, doi:10.1016/j.chemosphere.2004.08.055

Han, Y., Cao, X., Ouyang, X., Sohi, S. P., & Chen, J. (2016). Adsorption kinetics of magnetic biochar derived from peanut hull on removal of Cr (VI) from aqueous solution: Effects of production conditions and particle size. *Chemosphere*, *145*, 336–341. doi:10.1016/j.chemosphere.2015.11.050

Hao, Z., Wang, C., Yan, Z., Jiang, H., & Xu, H. (2018). Magnetic particles modification of coconut shell-derived activated carbon and biochar for effective removal of phenol from water. *Chemosphere*, *211*, 962-969. doi:10.1016/j.chemosphere.2018.08.038

He, R., Peng, Z., Lyu, H., Huang, H., Nan, Q., & Tang, J. (2018). Synthesis and characterization of an iron-impregnated biochar for aqueous arsenic removal. *Science of the Total Environment*, *612*, 1177–1186. doi:10.1016/j.scitotenv.2017.09.016

Hossain, A., & Aditya, G. (2013). Cadmium biosorption potential of shell dust of the fresh water invasive snail Physa acuta. *Journal of Environmental Chemical Engineering*, *1*(3), 574-580. doi:10.1016/j.jece.2013.06.030

Hossain, A., Bhattacharyya, S. R., & Aditya, G. (2015). Biosorption of cadmium from aqueous solution by shell dust of the freshwater snail Lymnaea luteola. *Environmental Technology & Innovation*, *4*, 82–91. doi:https://doi.org/10.1016/j.eti.2015.05.001

Hu, X., Xu, J., Wu, M., Xing, J., Bi, W., Wang, K., et al. (2017). Effects of biomass pre-pyrolysis and pyrolysis temperature on magnetic biochar properties. *Journal of Analytical and Applied Pyrolysis*, *127*, 196-202. doi:10.1016/j.jaap.2017.08.006

Huu Tap Van, Lan Huong Nguyen, Van Dang Nguyen, X. H. N., Thanh Hai Nguyen, Tien Vinh Nguyen, Saravanamuth Vigneswaran, J. R., & Tran, H. N. (2018). Characteristics and mechanisms of cadmium adsorption onto biogenic aragonite shells-derived biosorbent: Batch and column studies. *Journal of Environmental Management*, *241*, 535-548. doi.org/10.1016/j.jenvman.2018.09.079

Inyang, M. I., Gao, B., Yao, Y., Xue, Y., Zimmerman, A., Mosa, A., et al. (2016). A review of biochar as a low-cost adsorbent for aqueous heavy metal removal. *Critical Reviews in Environmental Science and Technology*,

46(4), 406–433. doi:10.1080/10643389.2015.1096880

Karimi, M., Shojaei, A., Nematollahzadeh, A., & Abdekhodaie, M. J. (2012). Column study of Cr (VI) adsorption onto modified silica–polyacrylamide microspheres composite. *Chemical Engineering Journal*, *210*, 280–288. doi:https://doi.org/10.1016/j.cej.2012.08.046

Khitous, M., Salem, Z., & Halliche, D. (2016). Effect of interlayer anions on chromium removal using Mg–Al layered double hydroxides: Kinetic, equilibrium and thermodynamic studies. *Chinese Journal of Chemical Engineering*, *24*(4), 433–445. doi:https://doi.org/10.1016/j.cjche.2015.11.018

Lu, J., Fu, F., Zhang, L., & Tang, B. (2018). Insight into efficient co-removal of Se(IV) and Cr(VI) by magnetic mesoporous carbon microspheres: Performance and mechanism. *Chemical Engineering Journal*, *346*, 590–599. doi:https://doi.org/10.1016/j.cej.2018.04.077

Mthombeni, N. H., Mbakop, S., Ray, S. C., Leswifi, T., Ochieng, A., & Onyango, M. S. (2018). Highly efficient removal of chromium (VI) through adsorption and reduction: A column dynamic study using magnetized natural zeolite-polypyrrole composite. *Journal of Environmental Chemical Engineering*, *6*(4), 4008-4017. doi:10.1016/j.jece.2018.05.038

Mthombeni, N. H., Onyango, M. S., & Aoyi, O. (2015). Adsorption of hexavalent chromium onto magnetic natural zeolite-polymer composite. *Journal of the Taiwan Institute of Chemical Engineers*, *50*, 242-251. doi:10.1016/j.jtice.2014.12.037

Nan, Z., Shi, Z., Yan, B., Guo, R., & Hou, W. (2008). A novel morphology of aragonite and an abnormal polymorph transformation from calcite to aragonite with PAM and CTAB as additives. *Journal of Colloid and Interface Science*, *317*(1), 77–82. doi:https://doi.org/10.1016/j.jcis.2007.09.015

Nguyen, L. H., Minh, T., Nguyen, P., Van, H. T., & Vu, X. H. (2019). Treatment of Hexavalent Chromium Contaminated Wastewater Using Activated Carbon Derived from Coconut Shell Loaded by Silver Nanoparticles : Batch Experiment. *Water, Air & Soil Pollution*, *230*, 68. doi.org/10.1007/s11270-019-4119-8

Rai, M. K., Shahi, G., Meena, V., Meena, R., Chakraborty, S., Singh, R. S., & Rai, B. N. (2016). Removal of hexavalent chromium Cr (VI) using activated carbon prepared from mango kernel activated with H_3PO_4. *Resource-Efficient Technologies*, *2*, S63–S70. doi:https://doi.org/10.1016/j.reffit.2016.11.011

Saha, P. Das, Dey, A., & Marik, P. (2012). Batch removal of chromium (VI) from aqueous solutions using wheat shell as adsorbent: process optimization using response surface methodology. *Desalination and Water Treatment*, *39*(1-3), 95-102. doi:10.5004/dwt.2012.2905

Shang, J., Pi, J., Zong, M., Wang, Y., Li, W., & Liao, Q. (2016). Chromium removal using magnetic biochar derived from herb-residue. *Journal of the Taiwan Institute of Chemical Engineers*, *68*, 289–294. doi:https://doi.org/10.1016/j.jtice.2016.09.012

Tizo, M. S., Blanco, L. A. V, Cagas, A. C. Q., Dela Cruz, B. R. B., Encoy, J. C., Gunting, J. V, et al. (2018). Efficiency of calcium carbonate from eggshells as an adsorbent for cadmium removal in aqueous solution. *Sustainable Environment Research*, *28*(6), 326–332. doi:https://doi.org/10.1016/j.serj.2018.09.002

Turan, P., Doğan, M., & Alkan, M. (2007). Uptake of trivalent chromium ions from aqueous solutions using kaolinite. *Journal of Hazardous Materials*, *148*(1–2), 56–63. doi:10.1016/j.jhazmat.2007.02.007

Wang, S., Tang, Y., Li, K., Mo, Y., Li, H., & Gu, Z. (2014). Combined performance of biochar sorption and magnetic separation processes for treatment of chromium-contained electroplating wastewater. *Bioresource*

Technology, *174*, 67–73. doi:https://doi.org/10.1016/j.biortech.2014.10.007

Wang, X. S., Chen, L. F., Li, F. Y., Chen, K. L., Wan, W. Y., & Tang, Y. J. (2010). Removal of Cr (VI) with wheat-residue derived black carbon: Reaction mechanism and adsorption performance. *Journal of Hazardous Materials*, *175*(1–3), 816–822. doi:10.1016/j.jhazmat.2009.10.082

Wang, X. S., Li, Z. Z., & Tao, S. R. (2009). Removal of chromium (VI) from aqueous solution using walnut hull. *Journal of Environmental Management*, *90*(2), 721–729. doi:https://doi.org/10.1016/j.jenvman.2008.01.011

Xu, J., Yin, Y., Tan, Z., Wang, B., Guo, X., Li, X., & Liu, J. (2019). Enhanced removal of Cr(VI) by biochar with Fe as electron shuttles. *Journal of Environmental Sciences*, *78*, 109–117. doi:https://doi.org/10.1016/j.jes.2018.07.009

Yang, Y., Chen, N., Feng, C., Li, M., & Gao, Y. (2018). Chromium removal using a magnetic corncob biochar/polypyrrole composite by adsorption combined with reduction: Reaction pathway and contribution degree. *Colloids and Surfaces A: Physicochemical and Engineering Aspects*, *556*, 201–209. doi:https://doi.org/10.1016/j.colsurfa.2018.08.035

Yuan, P., Fan, M., Yang, D., He, H., Liu, D., Yuan, A., et al. (2009). Montmorillonite-supported magnetite nanoparticles for the removal of hexavalent chromium [Cr(VI)] from aqueous solutions. *Journal of Hazardous Materials*, *166*(2-3), 821-829. doi:10.1016/j.jhazmat.2008.11.083

Zhang, X., Zhang, L., & Li, A. (2018). Eucalyptus sawdust derived biochar generated by combining the hydrothermal carbonization and low concentration KOH modification for hexavalent chromium removal. *Journal of Environmental Management*, *206*, 989–998. doi:10.1016/j.jenvman.2017.11.079

Zhao, B., Zhang, J. E., Yan, W., Kang, X., Cheng, C., & Ouyang, Y. (2016). Removal of cadmium from aqueous solution using waste shells of golden apple snail. *Desalination and Water Treatment*, *57*(50), 23987–24003. doi:10.1080/19443994.2016.1140078

Zhou, L., Liu, Y., Liu, S., Yin, Y., Zeng, G., Tan, X., et al. (2016). Investigation of the adsorption-reduction mechanisms of hexavalent chromium by ramie biochars of different pyrolytic temperatures. *Bioresource Technology*, *218*, 351–359. doi:https://doi.org/10.1016/j.biortech.2016.06.102

Zhou, X., Liu, Y., Zhou, J., Guo, J., Ren, J., & Zhou, F. (2018). Efficient removal of lead from aqueous solution by urea-functionalized magnetic biochar: Preparation, characterization and mechanism study. *Journal of the Taiwan Institute of Chemical Engineers*, *91*, 457–467. doi:https://doi.org/10.1016/j.jtice.2018.04.018